Corrugated Long-Period Fiber Gratings as Strain, Torsion, and Bending Sensors

Chunn-Yenn Lin, Lon A. Wang, *Associate Member, IEEE,* and Gia-Wei Chern

***Abstract*—We present a novel corrugated long-period fiber grating whose transmission spectra are highly sensitive to the applied tensile strain, torsion, and bending due to the periodical index modulation created and changed by these mechanic forces. The induced index modulation can also be experimentally characterized by using a built-in fiber Bragg grating (FBG). The long period fiber gratings possess the following unique properties when used as sensors. As a tensile strain sensor, its resonance loss varies but resonance wavelength remains stable. As a torsion sensor, the wavelength varies with the applied twist rate. As a bending sensor, the cladding-mode resonance grows with the bending curvature.**

***Index Terms*—Corrugated structure, fiber gratings, fiber sensors.**

I. Introduction

GRATING-BASED fiber sensors are simple and intrinsic and have all the advantages normally attributed to fiber sensors such as electrically passive operation, electromagnetic immunity, high sensitivity, and multiplexing capabilities [1]. Those based on the long-period fiber grating (LPFG) can couple light between the core mode and the cladding modes and are more sensitive to the environment than the others. Various applications in sensing temperature, strain, refractive index, or bending curvature using such LPFG-based sensors have been reported [2], [3]. However, some limitations, particularly in sensing strain and bending, may be imposed. For example, since the index modulation of a conventional LPFG made by photoexposure [4] or other means [5]–[7] is almost fixed, the strength of the cladding-mode resonance remains almost constant. Therefore, when the conventional LPFG is used as a strain sensor, the shift of resonant wavelength instead of the variation of transmission loss is usually used as measurant because the former is much more sensitive to strain than the latter [2]. Consequently, the conventional LPFG is not suitable for real-time strain sensing applications. Furthermore, when the conventional LPFG is used as a bending sensor, the constant reinforcement in mode coupling will be destroyed as the fiber is bent. Therefore, a large bending curvature may completely wash out the grating properties, causing the resonant loss to be attenuated and the resonance wavelength to be hard to define [3], [4] . Moreover, when the conventional LPFG is twisted, little index perturbation is induced because the fiber structure is uniform. Thus, a torsion sensor based on fiber gratings has not been reported so far.

In this paper, we describe a new type of LPFG made of a corrugated structure over which a periodical strain distribution is induced when an external mechanical force, such as tensile, or torsion, or bending, is applied because the induced strain fields are all structure-dependent. Owing to the photoelastic effect, the strain distribution will cause a periodical index variation, which may result in the mode coupling between the guided fundamental mode and the forward-propagating cladding modes. Because the induced index modulation will change with these mechanical forces, the resultant coupling strength and phase-matching condition become sensitive, which leads to various kinds of fiber sensors. For the first time (to the best of our knowledge), we experimentally demonstrate the unique characteristics of a corrugated LPFG under tensile strain, torsion, and bending, which exhibits advantages over the conventional LPFG. We also implant a uniform fiber Bragg grating (FBG) in the corrugated structure so that, by monitoring its reflection spectrum, the effect of corrugation on the core-mode coupling behavior can be unambiguously characterized. Our focus in this paper will be on the experimental verification and qualitative justification of their working mechanisms.

The rest of this paper is arranged as follows. Section II describes qualitatively the principle of operation of the corrugated LPFG as fiber sensors. In Section III, the experimental results of characterizing such sensors with different corrugated depths and in different resonant modes are reported. In Section IV, some working principles are qualitatively verified by measuring the evolution of reflection spectra from a built-in FBG in the corrugated structure. The measured sensitivities to tensile strain, torsion, and bending are demonstrated in Section V, followed by conclusions.

II. Principle of Operation

The LPFG made of a corrugated structure is schematically shown in Fig. 1. It consists of two unit sections. One is the etched region with cladding radius r_e and the other is the unetched region with radius r_u. The corrugated structure introduces a periodic change of index profiles along the longitudinal direction. However, this corrugated structure has little contribution to the mode couplings when there is no mechanical stress present. This is because the waveguide modes involved in power exchanges are the fundamental core mode and the first few cladding modes. These modes, whose effective indexes are close to the core index, are mainly confined within the central

Manuscript received May 9, 2000; revised April 30, 2001. This work was supported in part by the National Science Council under Contract 89-2213-E-002-199 and by the Education Ministry, Taiwan, R.O.C., under Contract 89E-FA06-2-4.

The authors are with the Department of Electrical Engineering and Institute of Electro-Optical Engineering, National Taiwan University, Taipei, Taiwan, R.O.C. (e-mail: lon@ccms.ntu.edu.tw).

Publisher Item Identifier S 0733-8724(01)06263-6.

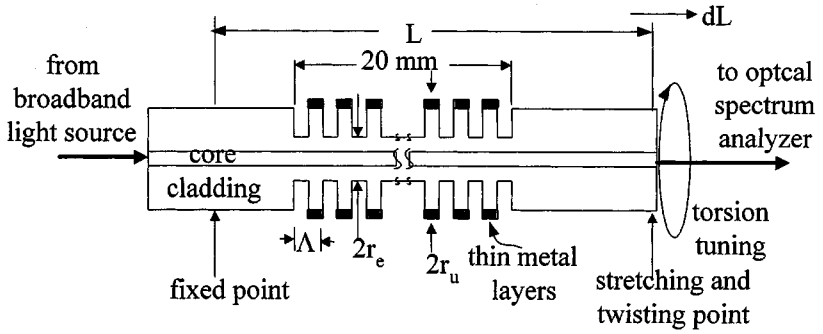

Fig. 1. Schematic diagram of a corrugated LPFG and its measurement setup.

region near the fiber core. For these centrally confined modes, the fields of the two regions are similar to each other for the same mode order. As a result, cross couplings through these discontinuities are insignificant due the smallness of the corresponding overlapping integrals. This can also be confirmed from the experimental observations in Sections III-A and IV, i.e., the resonant transmission loss of the device or the superstructure effect observed from a built-in FBG is almost negligible when no stress force is applied. The main mechanism accounting for the mode couplings is the periodic index perturbations, which are resulted from the differential strain fields within the corrugated structure through the photoelastic effect when external mechanical forces are applied. This is because when external stresses such as tensile, torsion, and bending are applied to the corrugated LPFG, the corresponding strain fields within the etched and the unetched regions are different. Because these photoelastic-induced index perturbations are functions of the applied forces, the coupling behaviors, such as resonant transmission losses or resonant wavelengths, are dependent on the applied stresses. This indicates that the corrugated LPFG can be used as potential mechanical sensors. We will discuss qualitatively, in the following subsections, the coupling performances for different kinds of applied stresses under the framework of coupled-mode theory.

A. Principle of Sensing Tensile Strain

First, we investigate the corrugated LPFG as a tensile strain fiber sensor. When a tensile force is applied to the corrugated LPFG, under the condition of mechanical equilibrium, the longitudinal forces are the same for the etched and unetched regions, which is equal to the applied force. The etched and unetched regions will, thus, experience different tensile stresses, which are inversely proportional to the cross-sectional areas of the corresponding region. By virtue of the photoelastic effect, the index changes of these two regions are therefore

$$\delta n_e(r) = -\frac{1}{2} p_e \left[n_e^{(0)}(r)\right]^3 \frac{F}{Y\pi r_e^2}, \qquad 0 \le r \le r_e$$

$$\delta n_u(r) = -\frac{1}{2} p_e \left[n_u^{(0)}(r)\right]^3 \frac{F}{Y\pi r_u^2}, \qquad 0 \le r \le r_u \quad (1)$$

where p_e is the effective photoelastic constant taking into account the effect of Poisson's ratio, Y is the Young's modulus, and $n_u^{(0)}(r)$ and $n_e^{(0)}(r)$ are the unperturbed index profiles of the unetched and etched regions, respectively. For the difference of the radii of these two regions, we see that there is a periodical index modulation induced by the tensile strain in the corrugated structure. The periodic index change has two components and can be written as follows:

$$\Delta n(r) = \Delta n_{\text{strain}}(r) + \Delta n_{\text{corrugated}}(r) \quad (2)$$

where one is strain dependent due to the photoelastic effect and the other is the intrinsically structural index changes between the two regions. The strain part is

$$\Delta n_{\text{strain}}(r) = \delta n_e(r) - \delta n_u(r) = -\frac{1}{2} p_e \left[n_e^{(0)}(r)\right]^3 \left[1 - \frac{r_u^2}{r_e^2}\right] s, \qquad 0 \le r \le r_e \quad (3)$$

where $s = F/(Y\pi r_u^2)$ is the induced tensile strain in the unetched region and the corrugated index change is

$$\Delta n_{\text{corrugated}}(r) = n_u^{(0)}(r) - n_{\text{sur}}, \qquad r_e \le r \le r_u \quad (4)$$

where n_{sur} is the index of surrounding media. Because, in general, the surrounding media is air and the radius contrast is large, the index difference in (4) cannot be treated as a perturbation to the cladding modes. A rigorous analysis for the corrugated structure can be developed based on the scattering matrix method or the transfer matrix method [8]–[10]. However, we will defer the rigorous analysis to a future publication and use the coupled-mode theory [11], [12] to qualitatively describe the operation of the corrugated LPFG as a sensing device. Because the core-mode field is highly confined in the core region, the periodic index changes in (4) has almost no effect on the core mode. However, the confinement of cladding modes is due to the cladding–surrounding interface, and the corrugated structure indeed influences the coupling behaviors through the tails of the cladding-mode fields. Because we are mainly concerned with couplings with core mode through the strain-induced index perturbation in (3), the interaction region is mainly concentrated near the core-mode area. Thus, as regards coupling descriptions, we may use some averaged cladding modes as the unperturbed fields with respect to the strain-induced Δn_{strain}. Let us define this averaged cladding mode as $\bar{\mathbf{e}}_{\text{cl}}$. Then the averaged, or empirical, coupling coefficient $\bar{\kappa}$ between core mode and cladding mode is defined as

$$\bar{\kappa} = \frac{\omega\varepsilon_0}{4} \int_{A_\infty} 2n_e^{(0)} \Delta n_{\text{strain}}(r) \mathbf{e}_{\text{co}}^*(r) \cdot \bar{\mathbf{e}}_{\text{cl}}(r) \mathrm{d}A. \quad (5)$$

Here, the mode fields are assumed to be normalized to carry unit power. Thus, as an empirical formula, we use this averaged coupling coefficient to express the transmission loss T of the corrugated LPFG for the core mode using

$$T \cong \cos^2(\bar{\kappa} l) = \cos^2\left[\alpha\left(\frac{r_u^2}{r_e^2}-1\right) s l\right] \tag{6}$$

where l is the length of the corrugated LPFG. In the second expression of (6), we introduce another empirical coefficient α. Here, α represents the overall dependence on the overlapping integrals and photoelastic constants. We also emphasize the dependence of transmission on measurable quantities, i.e., the applied tensile strain s, the total length l, and the difference of fiber-cladding areas. From this, we can see that the corrugated LPFG can act as strain fiber sensor by measuring the transmission loss of the core mode. The above expression indicates a cosine square dependence of the transmission on the tensile strain. As the radius contrast between the two regions increases, the sensitivity of the transmission loss on strain also increases, as can be seen qualitatively from (6). In addition, from (5), the loss sensitivity also depends on which cladding mode is being used. This modal dependence manifests itself through the empirical parameter α.

Based on the coupled-mode analysis, the resonance wavelength is determined by the following phase-matching condition [12]:

$$\begin{aligned} &2\delta_{\text{co-cl}} + \kappa_{\text{co}} - \bar{\kappa}_{\text{cl}} = 0 \\ &\kappa_r = \frac{\omega\varepsilon_0}{4}\int_{A_\infty} 2n_e^{(0)}\Delta n_{\text{strain}}(r)\mathbf{e}_r^*(r)\cdot\mathbf{e}_r(r)dA, \\ &\qquad\qquad r = \text{co or cl} \end{aligned} \tag{7}$$

where $\delta_{\text{co-cl}}$ is the detuning parameter. Because the index change is induced in the overall fiber profile, besides the self-coupling coefficient of the core mode κ_{co}, we have added a term accounting for the averaged self-coupling coefficient of cladding mode $\bar{\kappa}_{\text{cl}}$ in (7), which is important in our corrugated structure. (Compare with [12, Eq. (48)], which assumes that only the core mode is substantially affected owing to only the index in the core being changed.) Using the definition of detuning parameter, from [12], the above resonance condition can also be modified as

$$\lambda = \frac{\Lambda\left(n_{\text{co}} - \bar{n}_{\text{cl}}\right)}{1 + \left(\bar{\kappa}_{\text{cl}} - \kappa_{\text{co}}\right)\Lambda/2\pi} \tag{8}$$

where n_{co} is the core-mode effective index, $\bar{n}_{\text{cl}}$ is the averaged cladding-mode effective index, and Λ is the grating period. By (8), we will investigate the effects caused by the tensile strain, torsion, and bending on this phase-matching condition. First, we consider the changes due to tensile strain. The effective index of the two modes will be changed by the tensile strain due to the photoelastic effect, and in (7) and (8), these changes are taken into consideration by the two self-coupling terms κ_{co} and $\bar{\kappa}_{\text{cl}}$. Because the waveguide of a fiber is weakly guided and the strain-induced perturbation covers the whole cladding area, after normalization, the two self-coupling coefficients κ_{co} and $\bar{\kappa}_{\text{cl}}$ for tensile strain are approximately the same. As can be seen from (8), the overall shift of the resonance wavelength is expected to be smaller than that of the conventional LPFG during the growth of index modulation, as will be discussed in Section III-A.

B. Principle of Sensing Twist Rate

Next, we consider the effect caused by twisting the corrugated LPFG as a torsion sensor. As is well known, birefringence will be induced by twisting a fiber of uniform cross-section. However, because the fiber is weakly guided, the induced birefringence is approximately the same for the core mode and the cladding modes. Thus, the effects of torsion on the couplings between the core mode and the cladding modes through corrugated LPFG are our main concern here. For a uniform rod subject to an applied torque, the twist rate defined as the torsional angle per length between two ends is inversely proportional to the fourth power of the radius [14]. Thus, for our corrugated structure, another periodical index modulation apart from that caused by tensile strain is induced under twisting. However, the contribution is small compared to that from tensile strain. The main effect of torsion on the performance of couplings within the corrugated LPFG is to modify the phase-matching condition. The reason is as follows. As described previously, the twist rates are different in the etched and unetched regions due to the difference of the corresponding cladding radii. As a result, there will be significant excess stresses around the area near the etched cladding radius of the discontinuous conjunction when the fiber is under torsion. Because the corresponding strain fields are mainly distributed within the cladding region, from (7), these will contribute to the self-coupling term $\bar{\kappa}_{\text{cl}}$ of the cladding mode. In contrast, the contribution to κ_{co} for the core mode is much smaller due to the confinement of core-mode fields within the core. As a result, the torsion will shift the resonance wavelength to the shorter side [see (8)]. Owing to the similar values of κ_{co} and $\bar{\kappa}_{\text{cl}}$ caused by the tensile strain, it is expected that the resonance wavelength is almost dominated by the torsion effect when a tensile strain combined with torsion. From the above discussion and the characteristics of (7) and (8), the shift of peak resonant wavelength will increase with the applied torque. Thus, a novel torsion sensor based on the corrugated LPFG can be realized. An exact analysis of the strain fields under torsion is complicated; however, we expect that as the radius contrast between the two regions increases, the induced excess stresses due to the radius difference also become larger. The sensitivity of wavelength shifting will be enhanced. In addition, the torsion sensitivity depends on which cladding mode is being used because the more the mode field is distributed in the cladding region, the larger the $\bar{\kappa}_{\text{cl}}$ value will be.

To verify the changes of the core-mode self-couplings, a uniform photoinduced FBG is also built in the corrugated section of the fiber, and the photoinduced index change is concentrated within the fiber core. The FBG is designed to couple the forward-propagating core mode to the counter-propagating one when the phase-matching condition is satisfied [12]. When the corrugated LPFG is under external mechanical forces, the strain fields will induce a periodic change to the core-mode self-coupling κ_{co}. Due to the relatively large periodicity of LPFG, a FBG with superstructure modulation is created. Thus,

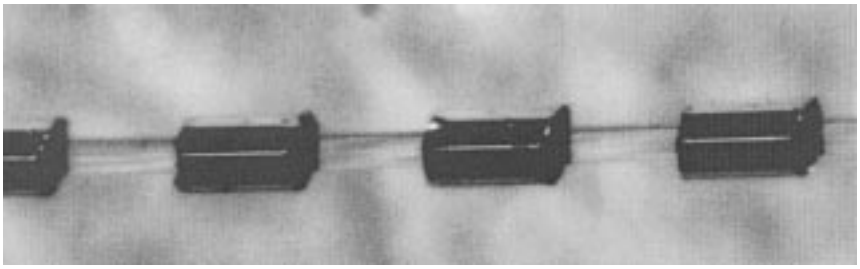

Fig. 2. Photomicrograph of corrugated fiber structure.

we can observe the changes of κ_{co} by monitoring the change of reflection spectrum from FBG, and the corresponding change of $\bar{\kappa}_{cl}$ can be deduced from (8).

C. Principle of Sensing Bending

From a mechanical analysis of simple bending, it is noted that when a torque applies to bend fiber, the resultant bending curvature is inversely proportional to the moment of inertia [15], [16]. For a uniform circular fiber with cladding radius r_{cl}, the moment of inertia can be expressed as $\pi r_{cl}^4/4$. Although the exact strain distribution of a corrugated fiber structure under bending requires sophisticated mechanical analysis due to the difference of cladding radius, the local bending curvature of the etched region is expected to be larger than that of the unetched region from the above discussion. Along the fiber axis, this difference will in turn create a periodic variation of strain field, and, thus, a periodic index perturbation owing to photoelastic effect. However, within the transverse plane of a uniform fiber, bending may cause an asymmetric strain distribution and thus result in an asymmetric index variation [17]. Therefore, the periodic index perturbation causes coupling from core mode to asymmetric cladding modes [18]. Because the resultant index perturbation increases with the applied torque, the resonance loss is expected to increase with the bending curvature. In addition, bending also changes the effective cladding-mode index, and thus modifies the phase-matching condition and causes the resonance wavelength to shift. Therefore, by monitoring the growth of mode coupling with bending curvature, the corrugated LPFG can also be used as a bending sensor.

III. Experiment Results and Discussion

A dispersion-shifted fiber (DSF) with an original cladding radius (r_u) of 62.5 μm is used. An evaporation system is used to deposit thin metal layers with a total thickness of $\sim$120 nm onto the fiber with a special setup to form a segmented ring pattern for etching protection. Thus, the corrugated structure is obtained by etching this prepatterned fiber in a hydrofluoric acid solution. The photomicrograph shown in Fig. 2 is a partial section of the corrugated LPFG, which has a period of $\sim$350 μm, a total length of 20 mm, and an etched diameter ($2r_e$) of $\sim$53 μm controlled by etching time.

The experiment setup for characterizing the corrugated LPFG as tensile strain or torsion sensor is also depicted in Fig. 1. A tensile force and an external torsion torque are applied to inducing an average tensile strain dL/L and an average twisting rate $\tau = 2\pi N/L$ (rad/m), respectively. dL and N are the total elongation and the number of torsional turns over the distance L between the fixed and the stretching points. To have a precise control on the adjustment of τ and dL/L, L is set as long as 1 m. Because L is much larger than the length of the etched region, the additional contributions of the elongation and the torsional angle to the measured dL/L and τ from the etched region are negligible. The value of dL/L and τ are, thus, approximately the same as those in unetched regions. A broadband light source and an optical spectrum analyzer are used for the measurement of spectral behaviors and power variations.

A. Characteristics of Sensing Tensile Strain

A typical spectral response of the corrugated LPFG under increasing applied strain dL/L is shown in Fig. 3. Two resonant coupling modes resulting from the corrugated LPFG are observed in the wavelength range, and their transmission losses at the resonance peaks increase with the applied strains as we expected in Section II-A. It should be noted that the spectrum shape of the resonance loss is different from that shown in our previous report [19]. The previous corrugated LPFG was buried with a short ultraviolet (UV)-induced FBG in the middle of the corrugated region, but no FBG is implanted in this work. The difference between our previous and current works is attributed to the existence of a buried FBG, which may affect LPFG's mode coupling because of an increase of UV-induced core index. Note that from Fig. 3, the peak resonant wavelengths are always obtained at the same fixed wavelength regardless of strain value. This characteristic is very distinct from the conventional LPFGs, which exhibit a considerable amount of wavelength shift during the growth of index modulation [13]. As indicated in (8), such a characteristic is attributed to the similar values of κ_{co} and $\bar{\kappa}_{cl}$ caused by tensile strain.

The measured dependence of transmission loss on tensile strain at different etched radii for the first and the second coupling modes is shown in Fig. 4(a) and (b). It is found that for the same mode coupling, the sensitivity of resonant transmission to tensile strain increases with etched depth. This verifies that the periodical index modulation induced by the tensile strain not only is proportional to the applied strain but also increases with the square of the radius contrast [see (6)]. As further strain is applied, however, the resonant losses of both modes decrease due to the reverse coupling from cladding modes to core mode, which is similar to the overexposure case, as commonly observed in the fabrication of photoinduced LPFGs. These phenomena characteristically agree very well with (6). In addition, comparisons of transmission variations between the first and the second resonant modes as shown in

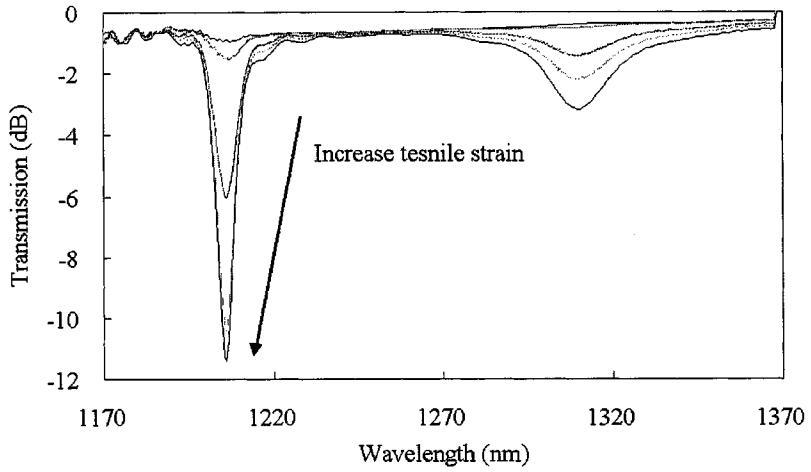

Fig. 3. Evolution of transmission spectra of a corrugated LPFG when tensile strains are applied.

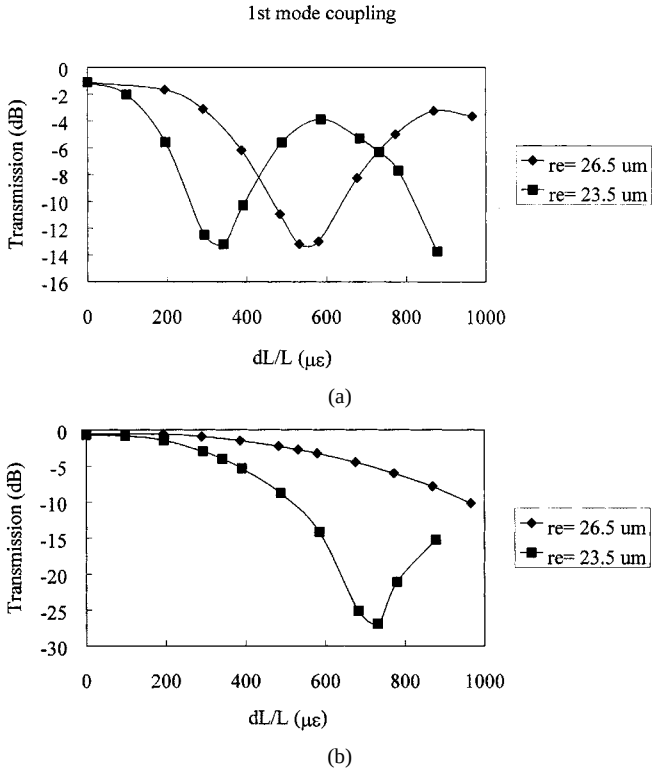

Fig. 4. Measured peak transmission loss versus applied tensile strains of the corrugated LPFGs with different etched radii for (a) first cladding resonance mode coupling and (b) second cladding resonance mode coupling.

Fig. 4 clearly indicate that when the first resonant mode is used as a strain sensor, a larger sensitivity will be obtained than when the second one is used. This can be understood as follows. For the DSF fiber we use, the overlapping integral between the core mode and the first cladding mode is larger than that between the core mode and the second cladding mode [see (5)], resulting in a larger $\bar{\kappa}$ in (6) for the first cladding mode. For verification, a conventional LPFG fabricated by UV exposure on the same kind fiber is used to study the overlapping strength of different cladding modes. Then, we find that indeed the growth of the first resonance is faster than that of the second one and is consistent with the previous reports [20], [21]. Therefore, for better sensitivity strain, it is better to measure the variation of the resonant loss resulting from the cladding mode (the first cladding mode for a DSF fiber), which has a larger overlapping integral with the core mode than the others.

B. Characteristics of Sensing Torsion

Fig. 3 shows that there is very weak resonant-mode coupling for a corrugated LPFG when neither tensile strain nor torsion is applied. This implies that to characterize the resonant wavelength shift owing to torsion effect as described in Section II-B, the corrugated LPFG needs to be loaded with a pretensile strain for an initial resonant-mode coupling. In measurements, the fiber is twisted by rotating one end with another end fixed. A typical spectrum evolution for the corrugated LPFG at increasing twist rates is shown in Fig. 5. Apart from the change in the resonant loss, the resonant wavelength shifts toward shorter wavelength sides, consistent with those described in Section II-B. Namely, it implies that the change of $\bar{\kappa}_{\mathrm{cl}}$ is larger than that of κ_{co}. An experiment proof of negligible change in κ_{co} caused by torsion will be described in Section IV. For comparison, we also do a similar torsion experiment on a conventional LPFG, and observe no obvious change in transmission spectrum even when the twist rate is increased to twice as large. Therefore, such a unique characteristic applicable as a torsion sensor is mainly attributed to the corrugated structure.

In Section II-B, we described that the shifting of peak resonant wavelength is dominated by the torsion effect. To verify it, we monitor the peak resonant wavelength at various twist rates but with increasing pretensile strain. The same behavior as shown in Fig. 3 is seen, i.e., the peak resonant wavelength remains stable at a fixed torsion rate but with various strains.

The variations of peak resonant wavelength with an applied twist rate at different etched radii for the first and the second mode couplings are shown in Fig. 6. It is found first that as the twist rate increases, the one with a smaller etched radius has a larger wavelength variation; secondly, for the same etched radius, the one using the second cladding mode coupling has a larger wavelength variation than the one using the first cladding mode coupling. The former phenomenon agrees well with Section II-B in that the sensitivity of the torsion sensor increases with the radius contrast. The latter can be explained as follows.

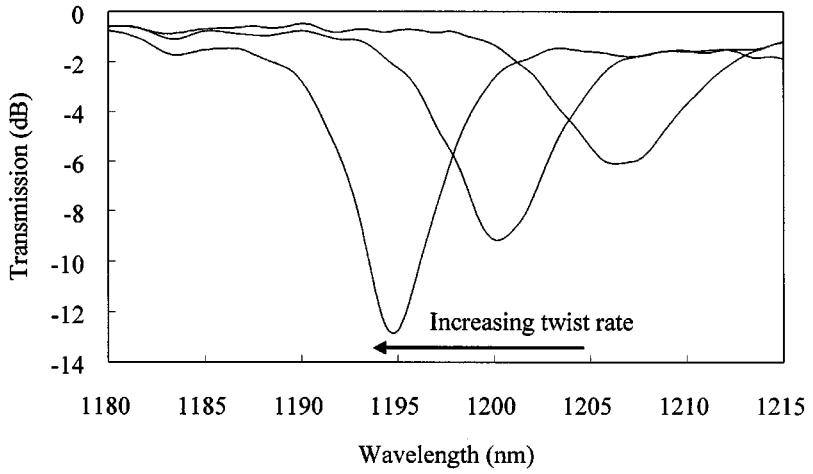

Fig. 5. Evolution of transmission spectra of the corrugated LPFG when twist rates are applied.

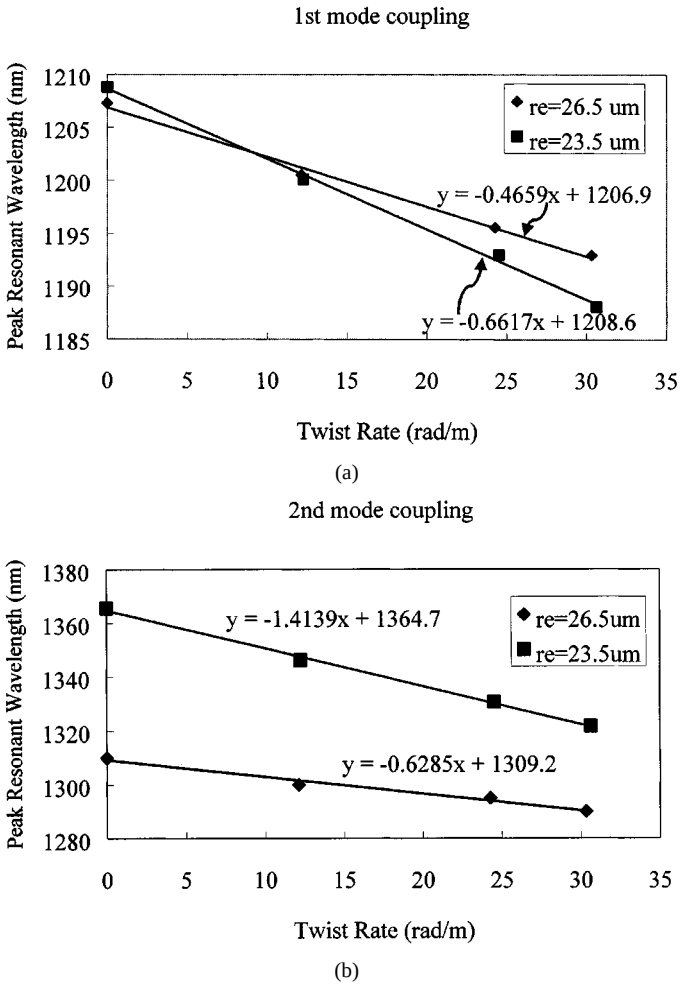

Fig. 6. Measured peak resonant wavelength versus applied twist rates of corrugated LPFGs with different etched radii for (a) first cladding resonance-mode coupling and (b) second cladding resonance-mode coupling.

The experimental result that the mode-coupling strength $\bar{\kappa}$ for the second cladding mode is weaker than that for the first one implies that the second cladding mode has a broader radial field distribution than that for the first cladding mode. And as described in Section II-B, the strain field induced by torsion is mainly distributed within the cladding region. As a result, the self-coupling coefficient $\bar{\kappa}_{cl}$ in (7) for the second cladding mode is larger and, thus, has more contribution to the wavelength shift than the first one does [see (8)]. Therefore, for the DSF fiber we use, it is shown that the second cladding mode can have a higher sensitivity to torsion effect. When the wavelength shift is used as an indicator for a torsion sensor, we conclude that it is more sensitive to the resonance of the cladding mode, which has a broader radial field distribution.

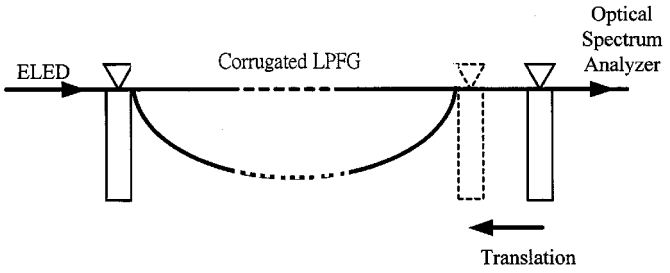

Fig. 7. Measurement setup for bending a corrugated LPFG.

C. Characteristics of Sensing Bending

An experiment setup similar to that described in [3] is utilized for characterizing a corrugated LPFG as bending sensor, and is shown in Fig. 7. A 45-cm-long fiber having a corrugated LPFG in the center is clamped between two stages without applied torsion. One stage is moved toward the other to induce bending, and the curvature obtained for a given translation is estimated by approximating the bent fiber as an arc of a circle, with the chord of the arc given by the translation stage separation.

A typical spectral response of the bending fiber sensor under the increasing bending curvature is shown in Fig. 8. Compared to the similar behaviors in [3] and [4] that bending a conventional LPFG could cause a resonant wavelength change and attenuation in mode-coupling strength, the effect of bending a corrugated LPFG is seen to accelerate the growth of mode coupling and, thus, to expedite the shifting of resonant wavelength toward the shorter wavelength side. These evolutions agree well

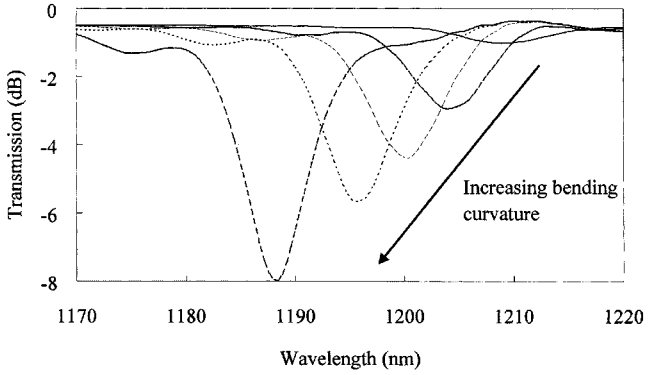

Fig. 8. Evolution of transmission spectra of a corrugated LPFG when bending curvatures are applied.

with Section III-C. Therefore, as a bending sensor, the corrugated LPFG can be used to detect bending curvature by measuring the difference of peak resonant wavelengths before and after bending.

IV. Characterization of Induced Index Modulation Using Built-In FBGs

To characterize the behaviors of mode couplings caused by tensile strain and torsion, we measure the reflection spectra of an FBG directly embedded in the same location as the corrugated structure to be formed. The weak and uniform FBG is ~7 mm, first imprinted by UV light exposure. Then, the corrugated structure is made and covers up the built-in FBG. The peak transmission loss of the FBG is set to be less than 2 dB so that the exposure-induced index modulation is negligibly small as compared to those caused by mechanical forces. Fig. 9(a)–(c) shows the evolution of reflection spectra when the corrugated LPFG is subject to various amounts of tensile strain without any torsion. When the built-in FBG is free and straight, the reflection spectrum shown in Fig. 9(a) is similar to a typical uniform FBG. It indicates that the effective index modulation induced by the corrugated waveguide structure is negligible. The evolution from Fig. 9(b) and (c) shows that as the applied tensile strain increases, the resonance wavelength shifts to the longer wavelength side with increasing sideband amplitudes. This can be understood as follows. A periodical strain modulation in the corrugated structure causes a periodical superstructure on the FBG with index and period modulations. The amplitudes of sidebands increase with the strength of periodical superstructure [22]. The spectral evolution of FBG shown in Fig. 9, therefore, provides direct evidence that a periodical index modulation is induced on the corrugated structure and increases with tensile strain, as expressed in (3).

Next, we show how the torsion affects the core mode by monitoring again the reflection spectra of FBG. Fig. 10 shows the evolution of reflection spectra when the corrugated LPFG is subject to various amounts of twist rates but with the tensile strain fixed, e.g., at 520 $\mu\varepsilon$ in this case. In contrast, no obvious difference among these FBG reflection spectra is observed, indicating that once the tensile strain is fixed, the core-mode coupling is essentially unaffected regardless of torsion effect. The same phenomenon is observed regardless of the amount

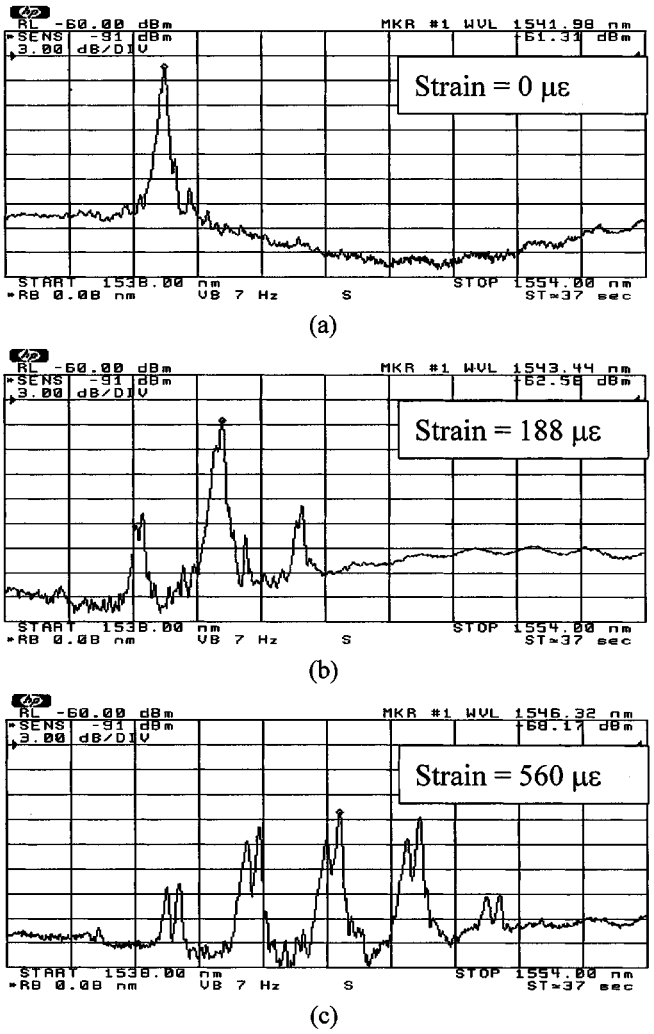

Fig. 9. Measured spectra of the built-in FBG without torsion but with various amounts of strain: (a) 0, (b) 188, and (c) 560 $\mu\varepsilon$.

of strain. However, it is noted from Section III-B that the measured wavelength shift of the corrugated LPFG as a torsion sensor does change over the torsion-tuning range. This clearly proves that the contribution of self-coupling of the core mode κ_{co} caused by the torsion effect is indeed negligible. It also implies that a considerable enhancement of $\bar{\kappa}_{\mathrm{cl}}$ caused by torsion is induced as expressed by (8).

V. Sensitivity of Corrugated LPFGs Used as Tensile Strain, Torsion, and Bending Sensors

A corrugated LPFG with ~350-μm period and ~21-μm etched radius is used as strain, torsion, and bending sensors. The fiber sensor has a first resonant-mode coupling at ~1211 nm when a tensile strain is applied. To measure the strain sensitivity, we increase the strain in a small step (~6 $\mu\varepsilon$) and measure the ratio of the transmitted power P_t to the initial power P_0 at the peak resonant wavelength. The measured result is shown in Fig. 11. A strain gauge factor, an indicator of sensor sensitivity, is defined as $(P_t - P_0)/(dL/L)$. The strain gauge factor is found to be ~5750 in the linear region, much larger than those reported before [2], [23].

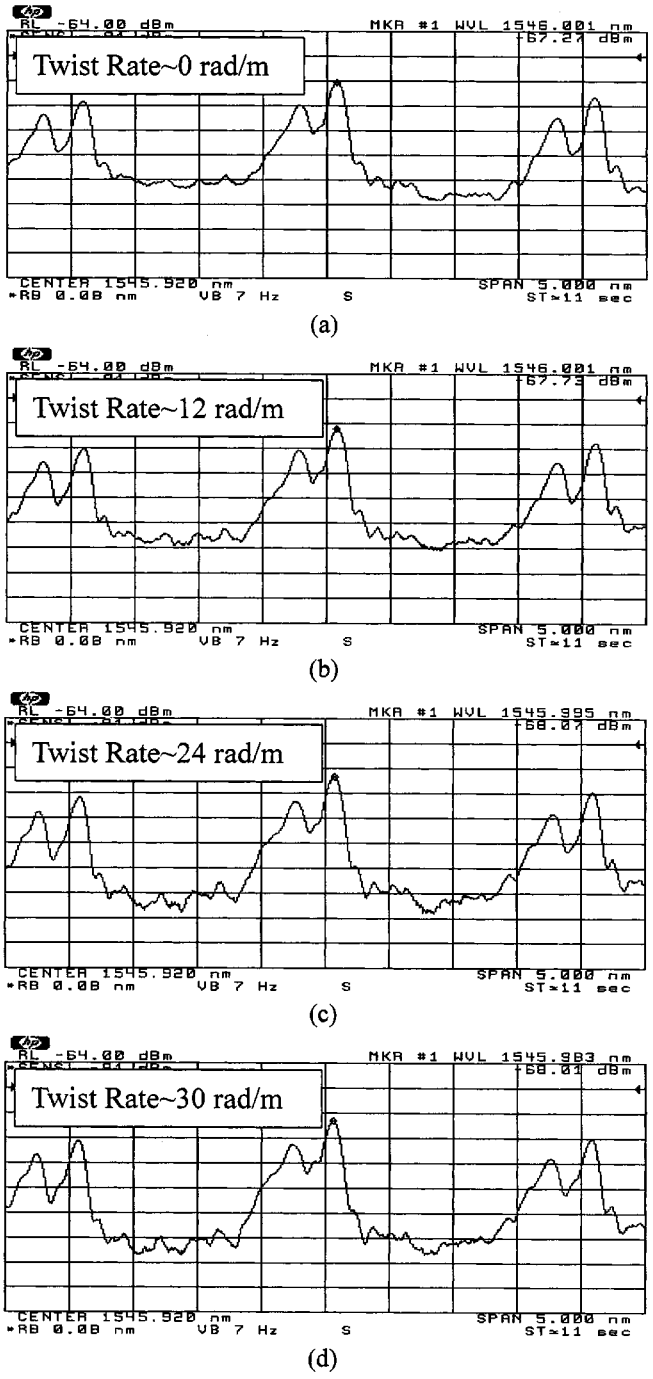

Fig. 10. Measured spectra of the built-in FBG at a fixed strain of 520 $\mu\varepsilon$ but with various amounts of twist rate: (a) 0, (b) 12, (c) 24, and (d) 30 rad/m.

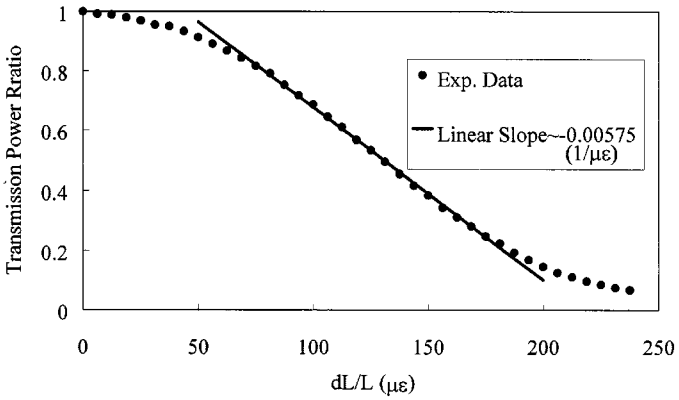

Fig. 11. Variation of transmitted power and linear sensitivity of the corrugated LPFG used as a strain fiber sensor.

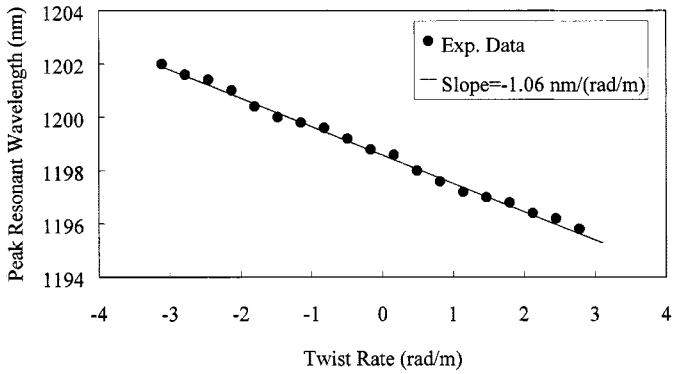

Fig. 12. Variation of peak resonant wavelength with clockwise and counterclockwise torsion and linear sensitivity of the corrugated LPFG used as a torsion sensor.

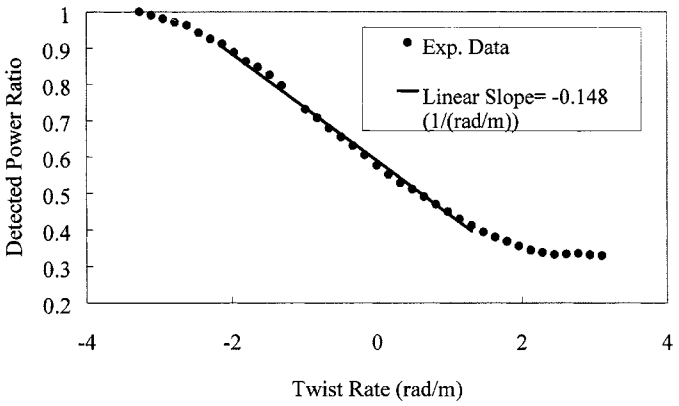

Fig. 13. Variation of transmitted power with clockwise and counterclockwise torsion and linear sensitivity of the corrugated LPFG used as potentially a real-time torsion sensor.

As for a torsion sensor, Section III-B shows that the peak resonant wavelength decreases with an increase in the amount of applied twist rate and nearly has nothing to do with the direction of applied torsion. However, in practice, it is important to distinguish between clockwise and counterclockwise torsions. To demonstrate that the torsion fiber sensor is also capable of sensing the direction of twist rate, we first apply a pretwist rate of ~14 rad/m on the fiber sensor with one end fixed; then, the other end is attached to the unit to be tested. As shown in Fig. 12, by measuring the peak resonant wavelength, a torsion sensor with a sensitivity of ~1.06 nm/(rad/m) is obtained. Note that, in practice, measuring the resonant wavelength change may not be suitable for real-time applications because of the time-consuming nature of scanning the spectra. To demonstrate that the torsion sensor can be used for such applications, monitoring of transmission power ratio at a fixed wavelength of ~1204 nm is utilized instead. The measured result is shown in Fig. 13, which has a fitting slope of -0.148 (rad/m)$^{-1}$ in the nearly linear region.

When the same corrugated LPFG is used as bending sensor, wavelength variation with bending curvature is shown in Fig. 14

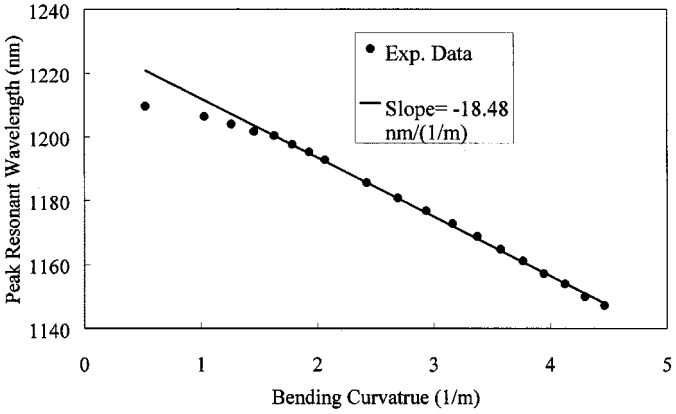

Fig. 14. Variation shift of peak resonant wavelength and linear sensitivity of the corrugated LPFG used as a bending sensor.

for curvatures ranging from 0.5 to 4.5 m^{-1}. A fitting slope of -18.48 nm/(m^{-1}) is obtained in the linear region. Note that when the bending curvature is small, the resonant band does not grow considerably, as shown in Fig. 8, and the peak resonant wavelength then becomes difficult to define and may result in a larger measurement error. Therefore, it is estimated the bending sensor can be applied to the measurement of curvature greater than 0.5 m^{-1} by current apparatus.

The temperature dependence of the same fiber sensor is measured and found to shift less than $+5$ nm per 100 °C, which is similar to that of a conventional LPFG [2]. The variation of resonant loss is also insensitive to the ambient temperature. These reveal that the thermal effect on the corrugated structure induces little extra index modulation owing to negligible dependence on the diameter of the fiber [24].

It should be mentioned that the measurement results on the sensitivities of strain, twist rate, and bending are repeatable, and no measurable hysteresis within the measuring ranges is found. After more than 50 times measurements on the same sensors, no measurable degradation is detected. For a pristine and unexposed fiber with cladding radius of 62.5 μm, it has been demonstrated to sustain an applied tensile stress of 930×10^6Pa without strength degradation [25]. Considering the stress ratio of the etched to unetched regions $(r_u/r_e)^2$ in a corrugated fiber, the allowable tensile stress is limited in the etched region. Thus, its corresponding allowable tensile force will be $\sim$1.3 N for a pristine and unexposed fiber with cladding radius of $r_e \sim 21$ μm. In our experiments assuming $Y = 7 \times 10^{10}$Pa, the allowable tensile force is up to $\sim$1 N without measurable degradation. Note that the fiber strength of our device is smaller than that of a pristine fiber, probably owing to the stress concentration or micro crack from etching; however, it may be improved by recoating materials such as polymer, metals, carbon, and diamond-like film.

VI. Conclusion

A novel LPFG composed of a corrugated structure that can be made by etching a fiber is proposed, and the behavior of the mode coupling is experimentally characterized for the first time. We have shown that owing to its novel corrugated structure, the corrugated LPFG can be used as strain, torsion, and bending sensors with unique sensing characteristics that have not been found in the conventional fiber sensor so far. As a tensile strain sensor, its peak resonant wavelength remains stable and its resonance loss is very sensitive to the applied tensile strain. As a torsion sensor, it is shown that the peak resonant wavelength decreases as the applied twist rate increases. To the best of our knowledge, this is the first fiber sensor ever reported whose transmission spectrum is directly sensitive to the applied twist rate. As a bending sensor, the cladding-mode resonance grows with increasing bending curvature rather than being attenuated as commonly observed in conventional LPFGs. Such unique characteristics may enable the corrugated LPFG-based fiber sensor to overcome the limitations of conventional fiber grating and to be suited for high-sensitive strain sensor, direct torsion sensor, and bending sensors for measuring large curvature. In addition, owing to the sensitivities of resonant loss and wavelength forces, various applications in optical communication are also expected.

References

[1] A. D. Kersey, M. A. Davis, H. J. Patrick, M. LeBlanc, K. P. Koo, C. G. Askins, M. A. Putnam, and E. J. Friebele, "Fiber grating sensors," *J. Lightwave Technol.*, vol. 15, pp. 1442–1463, Aug. 1997.

[2] V. Bhatia and A. M. Vengsarkar, "Optical fiber long-period grating sensors," *Opt. Lett.*, vol. 21, pp. 692–694, 1996.

[3] H. J. Patrick, C. C. Chang, and S. T. Vohra, "Long period fiber gratings for structural bend sensing," *Electron. Lett.*, vol. 34, pp. 1773–1775, Sept. 3, 1998.

[4] A. M. Vengsarkar, P. J. Lemaire, J. B. Judkins, V. Bhatia, T. Erodogan, and J. E. Spie, "Long-period fiber gratings as band-rejection filters," *J. Lightwave Technol.*, vol. 14, pp. 58–65, Jan. 1996.

[5] S. G. Kosinski and A. M. Vengsarkar, "Splicer-based long-period fiber gratings," in *Proc. OFC'98*, 1998, pp. 278–279.

[6] M. Akiyama, K. Nishide, K. Shima, A. Wada, and R. Yamauchi, "A novel long-period fiber grating using periodically released residual stress of pure-silica core fiber," in *Proc. OFC'98*, 1998, pp. 276–27.

[7] I. K. Hwang, S. H. Yun, and B. Y. Kim, "Long-period fiber gratings based on periodic microbends," *Opt. Lett.*, vol. 24, pp. 1263–1265, 2000.

[8] R. E. Collins, *Foundations for Microwave Engineering*. New York: McGraw-Hill, 1966.

[9] J. Pace and R. Mittra, "Generalized scattering matrix analysis of waveguide discontinuity problems," in *Quasi-Optics XIV*. New York: Polytechnic Inst. Brooklyn , 1964.

[10] G. W. Chern and L. A. Wang, "Transfer-matrix method based on perturbation expansion for periodic and quasiperiodic binary long-period gratings," *J. Opt. Soc. Amer. A*, vol. 16, pp. 2675–2689, 1999.

[11] D. Marcuse, *Theory of Dielectric Optical Waveguide*. Boston, MA: Academic, 1991.

[12] T. Erdogan, "Cladding-mode resonances in short- and long-period fiber grating filters," *J. Opt. Soc. Amer. A*, vol. 14, pp. 1760–1773, 1997.

[13] T. W. MacDougall, S. Pilevar, C. W. Haggans, and M. A. Jackson, "Generalized expression for the growth of long period gratings," *IEEE Photon. Technol. Lett.*, vol. 10, pp. 1449–1451, Oct. 1998.

[14] F. P. Beer and E. R. Johnston, *Mechanics of Materials*. Toronto, ON, Canada: McGraw-Hill Ryerson, 1985.

[15] F. L. Singer and A. Pytel, *Strength of Materials*, 3rd ed. New York: Harper & Row, 1980.

[16] S. Timoshenko and J. N. Goodier, *Theory of Elasticity*, 3rd ed. New York: McGraw-Hill, 1970.

[17] F. El-Diasty, "Multiple-beam Interferometric determination of Poission's ratio and strain distribution profiles along the cross section of bent single-mode fibers," *Appl. Opt.*, vol. 39, pp. 3197–3201, 2000.

[18] M. Vaziri and C. L. Chen, "An etched two-mode fiber modal coupling element," *J. Lightwave Technol.*, vol. 15, pp. 474–481, Mar. 1997.

[19] C. Y. Lin and L. A. Wang, "Loss-tunable long period fiber grating made from etched corrugation structure," *Electron Lett.*, vol. 35, pp. 1872–1873, Oct. 14, 1999.

[20] B. H. Lee and J. Nishii, "Cladding-surrounding interface insensitive long period fiber grating," *Electron Lett.*, vol. 34, pp. 1129–1130, May 28, 1998.

[21] H. J. Patrick, A. D. Kersey, and F. Bucholtz, "Analysis of the response of long period fiber grating to external index of refraction," *J. Lightwave Technol.*, vol. 16, pp. 1606–1612, Sept. 1998.
[22] W. F. Liu, P. St. J. Russell, and L. Dong, "100% efficient narrow-band acoustooptic tunable reflector using fiber Bragg grating," *J. Lightwave Technol.*, vol. 16, pp. 2006–2009, Nov. 1998.
[23] V. Grubsky and J. Feinberg, "Long-period fiber gratings with variable coupling for real-time sensing applications," *Opt. Lett.*, vol. 25, pp. 203–205, 2000.
[24] M. Song, B. Lee, S. B. Lee, and S. S. Choi, "Interferometric temperature-insensitive strain measurement with different-diameter fiber Bragg gratings," *Opt. Lett.*, vol. 22, pp. 790–792, 1997.
[25] R. Feced, M. P. Roe-Edwards, S. E. Kanellopoulos, N. H. Taylor, and V. A. Handerek, "Mechanical strength of degradation of UV exposed optical fibers," *Electron Lett.*, vol. 33, pp. 157–158, Jan. 16, 1997.

Chunn-Yenn Lin, photograph and biography not available at the time of publication.

Lon A. Wang (M'95–A'96), photograph and biography not available at the time of publication.

Gia-Wei Chern, photograph and biography not available at the time of publication.